Mon. Not. R. Astron. Soc. **306,** 684–690 (1999)

Effects of gravity on the structure of post-shock accretion flows in magnetic cataclysmic variables

Mark Cropper,[1] Kinwah Wu,[2] Gavin Ramsay[1] and Aysegul Kocabiyik[1]
[1]*Mullard Space Science Laboratory, University College London, Holmbury St. Mary, Surrey RH5 6NT*
[2]*Research Centre for Theoretical Astrophysics, Department of Physics, Sydney University, Sydney NSW, Australia*

Accepted 1999 February 15. Received 1999 February 5; in original form 1998 October 23

ABSTRACT

We calculate the temperature and density structure of the hot post-shock plasma in magnetically confined accretion flows, including the gravitational potential. This avoids the inconsistency of previous calculations which assume that the height of the shock is negligible. We assume a stratified accretion column with 1D flow along the symmetry axis. We find that the calculations predict a lower shock temperature than previous calculations, with a flatter temperature profile with height. We revise previous determinations of the masses of the white dwarf primary stars, and find that for higher mass white dwarfs there is a general reduction in derived masses when the gravitational potential is included. This is because the spectrum from such flows is harder than that of previous prescriptions at intermediate energies.

Key words: accretion, accretion discs – methods: data analysis – stars: fundamental parameters – novae, cataclysmic variables – white dwarfs – X-rays: stars.

1 INTRODUCTION

Magnetic cataclysmic variables (mCVs) are strong emitters of hard X-rays. These are produced in the post-shock region immediately above the accreting white dwarf. In this post-shock region there is a strong temperature gradient between the shock front ($> 10^8$ K) and the surface of the white dwarf. By correctly modelling the properties of the emission region it is possible to determine fundamental proporties of the mCV, such as the mass of the white dwarf. For an overview of the modelling the hard X-ray emission see Cropper, Wu & Ramsay (1999), while Cropper (1990) and Warner (1995) provide more general reviews of mCVs.

Wu (1994; see also Wu, Chanmugam & Shaviv 1994) described a closed integral solution for the temperature and density profile of this post-shock flow. The treatment included cyclotron cooling as well as thermal bremsstrahlung: cyclotron cooling is important for those mCVs with strongly magnetic (> 10 MG) white dwarfs. The advantage of this scheme is that the temperature and density profiles can be calculated analytically (with the exception of a final summation). Thus multitemperature spectra can be calculated sufficiently rapidly to permit spectral fits to X-ray data. Previously, an analytical solution existed only for the pure bremsstrahlung case (Aizu 1973). The assumptions for the boundary conditions in Wu (1994) are the same as those in Aizu (1973): these are a cold pre-shock flow (at free-fall pre-shock velocities) followed by a strong shock and then a hot post-shock flow cooling on to a cold white dwarf surface (reaching zero temperature and velocity at the base of the flow). As in Aizu (1973), the height of the shock was assumed to be negligible, so that the effects due to gravity were neglected.

Cropper, Ramsay & Wu (1998) and Ramsay et al. (1998) used the Wu (1994) formulation to determine the masses of the white dwarfs in those mCVs observed with *Ginga*. The masses they derived are at the higher end of expectations and, in the case of XY Ari, are significantly higher than the best determinations obtained by other means (Ramsay et al. 1998). This indicates that there is more hard X-ray flux than expected, or less soft X-ray flux as a result of significantly more complex forms of absorption than assumed in Cropper et al. (1998). The latter has been explored for BY Cam in Done & Magdziarz (1998). The effect of absorption in mCVs is a topic of its own, and we do not pursue it here. Issues of the emission from a *structured* accretion region can be dealt with to first order by the summation of a sufficiently large number of local models with different accretion rates and magnetic fields. This is because the emission from the post-shock flow is optically thin in the continuum down to almost the white dwarf surface. Therefore, here we take the path of exploring the effect of reducing the restrictiveness of the assumptions in the emission model itself.

Several options present themselves at this stage. These include improvement of the lower boundary condition to match the atmosphere of the white dwarf more appropriately, separate treatment of the proton and electron populations, and more detailed treatment of the physics within the shock itself. It should be noted that there have been a number of calculations for the post-shock radial flows on to white dwarfs (e.g. Imamura & Durisen 1983, and references therein; Woelk & Beuermann 1996). Some of these include two-fluid effects, Compton cooling and the effect of a gravitational potential. These are all important. The aim of those calculations has been to determine the post-shock temperature and density, and to predict spectra and X-ray light curves, but they are unsuitable for the iterative model fitting of X-ray data. This differs from the

approach adopted by Wu (1994) and Cropper et al. (1998), which attempts to extract information from the X-ray spectra and which requires a formulation that can be computed sufficiently rapidly for that purpose. Here we continue along the path of improvements to that technique by addressing the elimination of a negligible shock height assumption. In so doing, we explore and elucidate clearly for the first time the effects of including a radially varying gravitational acceleration on the post-shock flow structure.

The justification for assuming that the shock height has negligible effect is given, for example, in Frank, King & Raine (1992). This is adequate for the first generation of mass estimates as in Cropper et al. (1998): however, in those cases where the cyclotron cooling is insignificant (the IPs) and where the mass of the white dwarf is larger than $\sim$0.8 $M_\odot$, application of the Aizu (1973) or Wu (1994) formulae results in very significant shock heights for typical specific accretion rates (0.3 $R_{\rm WD}$ for a 1.0-$M_\odot$ white dwarf accreting at 1.0 g s^{-1} cm^{-2}). This is inconsistent with the assumptions used by Aizu (1973), Wu (1994) and Cropper et al. (1998) (where the gravitational acceleration is ignored) and with Woelk & Beuermann (1996) (who use a constant gravitational acceleration). Since the temperature in the immediate post-shock region is the pre-shock velocity at that height (divided by a factor of 4 because of the strong shock jump condition), this implies that the shock temperature will be significantly lower than that calculated from the free-fall velocity *at the surface* as used when assuming a negligible shock height. For this paper we have therefore augmented the treatment in Wu (1994) to include the effect of the variation of the gravitational acceleration within the post-shock flow.

2 FORMULATION

We derive the following set of 1D steady state conservation equations taking into account the gravitational potential (see Appendix A for details):

$$\frac{\rm d}{{\rm d}x}(\rho v) = 0, \tag{1}$$

$$\frac{\rm d}{{\rm d}x}(\rho v^2 + P) = \frac{-GM\rho}{x^2}, \tag{2}$$

$$v\frac{{\rm d}P}{{\rm d}x} + \gamma P\frac{{\rm d}v}{{\rm d}x} = -(\gamma - 1)\Lambda. \tag{3}$$

With the ideal-gas law, $P/\rho = kT/\mu m_{\rm H}$, this set of equations is closed. Here x is the spatial coordinate, ρ is the density, v is the flow velocity, P is the pressure, γ is the adiabatic index, T is the temperature, μ is the mean molecular mass, and $m_{\rm H}$ is the mass of a hydrogen atom. Λ is the cooling term, which includes both bremsstrahlung and cyclotron radiation (Wu 1994), G is the constant of gravitation, and M is the mass of the white dwarf. We have included in Appendix A the derivation of the form of the Λ term (used but not shown in Wu 1994) for the reader to assess the treatment of the cyclotron cooling. Note that we limit ourselves strictly to a 1D flow: we do not for this work consider spherically symmetric accretion or accretion in a dipolar field geometry, as the form of (1) is particularly useful for our purposes.

The temperature and density structure of the post-shock flow can be computed from the coupled pair of non-linear first-order ODEs derived in Appendix A. Rapid increases in the density at base of the flow make it more advantageous to integrate using the velocity v as the independent variable: (A9) should therefore be inverted, and then the dependence for the composite variable ξ (see Appendix A) can be written in terms of the product of (A8) with the inverse of (A9). We therefore have

$$\frac{{\rm d}x}{{\rm d}v} = \frac{\gamma(\xi - v) - v}{-(\gamma - 1)\frac{AC}{v^2}\sqrt{v(\xi - v)}\left[1 + \epsilon_{\rm s}\frac{4^{\alpha+\beta}}{3^\alpha}\frac{(\xi - v)^\alpha v^\beta}{v_{\rm a}^{\alpha+\beta}}\right] + \frac{GM}{x^2}} \tag{4}$$

and

$$\frac{{\rm d}\xi}{{\rm d}v} = \frac{{\rm d}\xi}{{\rm d}x}\frac{{\rm d}x}{{\rm d}v} = -\frac{GM}{x^2 v}\frac{{\rm d}x}{{\rm d}v}. \tag{5}$$

Here $-C$ is the mass transfer rate, $v_{\rm a} = 4v_{\rm s}$ is the free-fall velocity at the height of the shock, A is the coefficient for bremsstrahlung radiation, $\alpha = 3.85$ and $\beta = 2$ are the coefficients corresponding to cyclotron radiation in Wu, Chanmugam & Shaviv (1994), and $\epsilon_{\rm s}$ is the ratio of the bremsstrahlung to cyclotron cooling time at the shock, as in Wu (1994).

Such a coupled system requires two boundary values. Unfortunately, this is not an initial-value problem: the initial value $x = R_{\rm WD}$ at $v = 0$ is known, but the variable ξ is not – it is constrained at the shock front by the requirement that the pressure immediately behind the shock $P_{\rm s} = 3Cv_{\rm a}/4$. Moreover, this is a floating boundary condition as the free-fall velocity $v_{\rm a}$ at the height of the shock is itself a result of the computation.

We have also combined the coupled pair (4 and 5) into a single second-order non-linear ODE in $x(v)$ (A14). Formally this now becomes an initial-value problem as at $x = R_{\rm WD}$, $v = 0$ (as above) and ${\rm d}v/{\rm d}x = \infty$. However, because of poles in (A14), neither of these are accessible. Step sizes must be chosen appropriately in order to maintain the stability of the integration, and this route therefore appears to provide no computational advantage at this stage.

3 IMPLEMENTATION

We have used a Runge–Kutta–Merson method in a shooting and matching technique implemented in the NAG D02HBF routine (Numerical Algorithms Group 1995) for floating boundary conditions to solve the coupled pair of equations 4 and 5. Initial guesses for the parameters of the routine are derived from the zero-gravity case. Convergence is generally reached within a few iterations, thus permitting a rapid calculation of the post-shock structure. The additional computation time overhead by comparison with the closed integral form in Wu (1994) is negligible.

We show in Fig. 1 the temperature and density profile of the post-shock flow for the zero-gravity case and our revised case including the gravitational potential. We assume a 1-$M_\odot$ white dwarf accreting at 1 g s^{-1} cm^2, corresponding to an accretion rate of $\sim 4 \times 10^{15}$ g s^{-1} over a fraction $f = 0.001$ of the white dwarf, typical for mCVs. The 0-MG, zero-gravity case is the standard Aizu profile, while the 30-MG zero-gravity case is the same as the Wu (1994) profile.

The effect of treating the gravitational potential more appropriately is significant, especially in the case of the pure bremsstrahlung cooling (0-MG field). The shock temperature is lower than that calculated from the Aizu profile, because the pre-shock velocities at this height are less than those at the surface of the white dwarf. However, there is significant heating of the post-shock flow itself through the release of gravitational potential energy, so the temperature in the subsequent flow is higher than that calculated from the Aizu profile. This leads to a flatter profile. In the case where we include cyclotron cooling from a 30-MG field, the correction is not so significant, as the height of the shock is in any case lower.

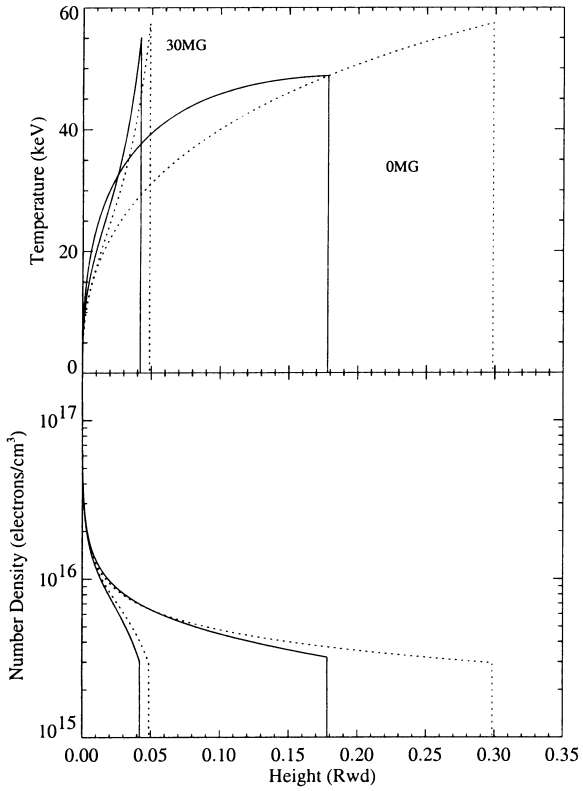

Figure 1. Upper plot: the temperature profile for the case including the gravitational potential (solid line) compared to the standard zero-gravity profile (dotted line) when cyclotron cooling is included (30 MG) and negligible (0 MG); the vertical lines are at the position of the shock front. Lower plot: as above, but for the electron number density profiles; see text for details.

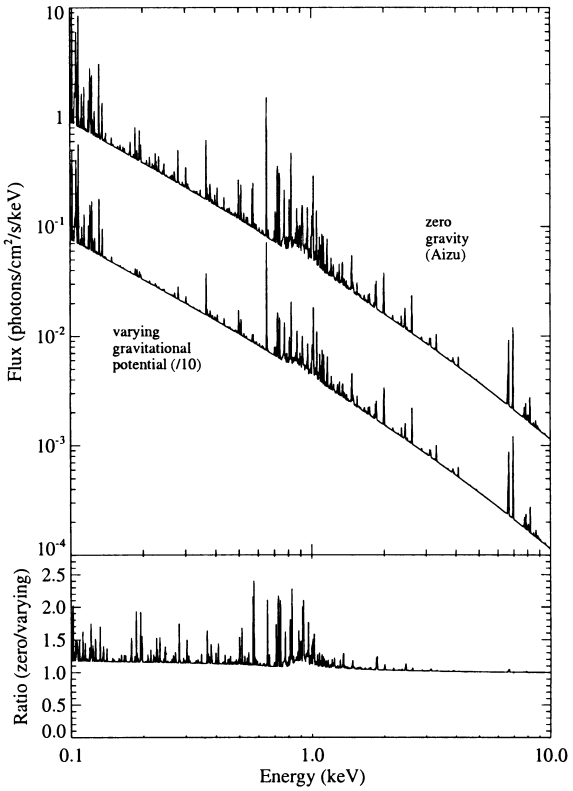

Figure 2. Upper panel: the photon spectrum from the Aizu profile (above), and, displaced downwards by a factor of 10 for clarity, that for the case when the effects of gravity are included. The parameters in Figure 1 are assumed here, and the system distance is 100 pc. Lower plot: the ratio of the Aizu spectrum to the spectrum from the varying gravitational potential.

In Fig. 2 we show the spectra for the pure bremsstrahlung case. The ratio plot (lower panel) indicates that the new profile produces a harder spectrum with fewer lines, at least for the 0.1 to 10 keV range shown here. This means that fits to X-ray data using the new profile will, somewhat counterintuitively, produce masses for the white dwarf which are lower than those determined using the Aizu (1973) or Wu (1994) profiles (Cropper et al. 1998).

At higher energies, the Aizu spectrum becomes harder, as the post-shock flow immediately behind the shock is at a higher temperature. However, because for 1-$M_\odot$ white dwarfs the shock temperature is $\sim$50 keV, this is somewhat higher than the typical range sampled by typical data sets available for these systems at present.

4 IMPROVED FITS TO DATA

Cropper et al. (1998) and Ramsay et al. (1998) derived masses for the accreting magnetic white dwarfs in the *Ginga* archives. Some of these exceeded 1.0 $M_\odot$. This indicates that the shock height in these particular systems is likely to be significant, especially for the intermediate polars in the sample. Therefore their white dwarf mass determinations can be improved significantly by taking into account the revised temperature and density profiles calculated above.

We have proceeded as in Cropper et al. (1998) and Ramsay et al. (1998), so that a direct comparison can be made with the earlier mass derivations. The results are shown in Table 1 for the former paper, and in Table 2 for the latter. An intermediate level of refinement is also shown in the tables: the earlier papers assumed a pure hydrogen plasma ($\mu = 0.5$) for calculating the temperature and density profiles of (but not the spectra from) the post-shock flow. Tables 1 and 2 therefore show the original mass determinations, the revised determinations with a cosmic plasma where $\mu = 0.615$, and then the present calculations including the gravitational potential and $\mu = 0.615$.

In addition to cold interstellar absorption, Cropper et al. (1998) and Ramsay et al. (1998) used a partially ionized absorber to account for the absorption within the system of the pre-shock flow. In the presence of density inhomogeneities in the accretion flow, and arc-shaped accretion footprints, the treatment of the absorption is a complex matter (Done & Magdziarz 1998; Rainger, in preparation). The final ingredients for the absorption model would include ionized absorption for the finely divided flow and a range of partial covering fractions for the density inhomogeneities, all integrated over a range of path-lengths dependent on the viewing angle to the flow. As noted earlier, this is beyond the scope of this work. However, we have included in Table 1 a final column which shows the fits including the gravitational potential and $\mu = 0.615$, but now assuming a partial covering of cold material rather than the partially ionized absorber. This may be useful for comparison with other workers, as the partially ionized absorber model is not generally available.

As expected from Figs 1 and 2, the results in Tables 1 and 2 indicate reduced masses for the massive white dwarfs in these systems when the gravitational potential is included in the shock structure. In the case of Table 1, the average (unweighted) reduction

Table 1. The best fit to the mass of the white dwarf in the magnetic CVs which were observed by *Ginga* using variants of the stratified accretion column model of Cropper et al. (1998). The upper panel shows the results of the synchronous (or very near) systems (the polars), while the lower panel shows the results of the asynchronous systems (the intermediate polars). The column with the mean molecular mass of the plasma, $\mu = 0.5$, corresponds to that assumed in Cropper et al. (1998). (Some of these new values differ marginally to those quoted there, since in this paper the accretion shock has been divided into 100 vertical elements as opposed to 50 there.) The remaining columns assume $\mu = 0.615$, with the last two columns including the gravitational term described in this paper (+G). IA refers to an ionized absorber, while PC refers to partial covering of cold absorber. The range in mass is the 90 per cent confidence interval. In all cases a cold absorber (for interstellar absorption) and a fluoresence line fixed at 6.4 keV have been included.

System	$\mu = 0.5 + \mathrm{IA}$ $\mathrm{M}_\odot(\chi^2_{\mathrm{red}})$	$\mu = 0.615 + \mathrm{IA}$ $\mathrm{M}_\odot(\chi^2_{\mathrm{red}})$	$\mu = 0.615 + \mathrm{G} + \mathrm{IA}$ $\mathrm{M}_\odot(\chi^2_{\mathrm{red}})$	$\mu = 0.615 + \mathrm{G} + \mathrm{PC}$ $\mathrm{M}_\odot(\chi^2_{\mathrm{red}})$
AM Her	1.22 (1.43: 1.15–1.30)	1.12 (1.28: 1.06–1.20)	1.06 (1.35: 0.97–1.16)	0.85 (0.61: 0.76–0.90)
EF Eri	0.88 (1.00: 0.82–0.94)	0.81 (1.07: 0.76–1.15)	0.80 (1.02: 0.75–0.85)	0.80 (0.91: 0.68–1.17)
BY Cam	1.08 (1.53: 1.00–1.25)	1.27 (1.43: >0.63)	1.18 (1.38: 0.76–1.27)	0.98 (1.16: >0.65)
V834 Cen	0.5 (0.88: 0.25–1.00)	0.5 (0.82: <1.3)	0.64 (0.89: <1.15)	0.54 (0.95: <1.25)
QQ Vul	1.13 (1.40: 0.95–1.30)	1.30 (1.32: >0.7)	0.95 (1.27: >0.6)	0.60 (1.18: 0.4–1.4)
EX Hya	0.52 (0.65: 0.42–0.60)	0.45 (0.59: 0.32–0.52)	0.50 (0.59: 0.44–0.56)	0.46 (0.56: 0.42–0.50)
AO Psc	0.40 (0.93: <0.80)	0.45 (0.90: <0.62)	0.36 (0.89: <0.65)	0.56 (0.94: 0.36–0.72)
FO Aqr	1.22 (0.83: >1.00)	1.12 (0.77: >0.89)	1.07 (0.73: 0.91–1.22)	0.92 (0.73: 0.58–1.22)
TV Col	1.20 (0.84: >0.95)	1.22 (0.93: 1.03–1.36)	1.21 (0.82: >1.06)	1.3 (1.21: >0.9)
BG CMi	1.25 (0.62: 1.05–1.39)	1.36 (0.93: >1.18)	1.19 (0.95: >0.95)	1.09 (0.58: >0.94)
TX Col	0.55 (1.34: 0.44–0.64)	0.48 (1.28: 0.41–0.54)	0.48 (1.23: 0.37–0.53)	0.48 (1.26: 0.39–0.54)
PQ Gem	1.35 (1.08: > 1.05)	1.32 (1.04: >1.15)	1.21 (1.06: >1.08)	1.29 (1.04: >1.17)
AE Aqr	0.3 (0.76: <1.15)	0.62 (0.68: 0.4–1.15)	0.6 (0.69: <1.0)	0.6 (0.66: <1.0)

in mass of those systems above 1.0 $\mathrm{M}_\odot$ in Cropper et al. (1998) is approximately 0.1 $\mathrm{M}_\odot$. For those below 1.0 $\mathrm{M}_\odot$, the masses are slightly ($\sim$0.03 $\mathrm{M}_\odot$) increased. There is little difference between the masses assuming $\mu = 0.5$ and $\mu = 0.615$ in the zero-gravity case. There is some scatter in the trends, because the fitting routine optimizes parameters such as mass transfer rate in addition to the white dwarf mass, and in some cases new global optima are found. The masses derived using the partial fraction covering model for the absorption are slightly lower still: for those systems previously above 1.0 $\mathrm{M}_\odot$ the average reduction in mass is a further $\sim$0.12 $\mathrm{M}_\odot$, while that for the less massive systems is unchanged.

In the case of Table 2, we also see reductions $\sim$0.1 $\mathrm{M}_\odot$, as the effect of the gravitational potential is included in the mass determinations for XY Ari.

5 CONCLUSIONS

The results in Tables 1 and 2 show a reduction in the mean of the derived masses for the white dwarf when the effects of gravity are included. The reductions are greatest for more massive white dwarfs, low specific accretion rates and low magnetic fields, because the shock height is greater under these conditions. The

Table 2. A comparision of mass estimates from XY Ari data using the models described in Table 1. No iron fluorescence component at 6.4 keV has been added. The range in mass is for the 90 per cent confidence level. The data in the first column have previously been reported in Ramsay et al. (1998).

Satellite	$\mu = 0.5 + \mathrm{IA}$ $\mathrm{M}_\odot$ (χ^2_{red})	$\mu = 0.615 + \mathrm{IA}$ $\mathrm{M}_\odot$ (χ^2_{red})	$\mu = 0.615 + \mathrm{IA} + \mathrm{G}$ $\mathrm{M}_\odot$ (χ^2_{red})
RXTE			
(1)	1.03 (1.04: 0.94–1.11)	0.98 (1.04: 0.85–1.03)	0.89 (1.04: 0.84–1.00)
(2)	0.89 (0.76: 0.83–1.02)	0.83 (0.76: 0.75–0.92)	0.82 (0.76: 0.74–0.91)
ASCA			
(GIS2)	1.05 (0.88: 0.81–1.32)	1.01 (0.88: 0.75–1.25)	0.96 (0.89: 0.72–1.16)
(GIS3)	1.38 (1.06: >1.18)	1.37 (1.07: >1.12)	1.25 (1.08: 1.05–1.36)
(GIS2&3)	1.25 (0.97: 1.08–1.38)	1.23 (0.97: 0.98–1.36)	1.15 (0.98: 0.96–1.25)
(SIS0)	1.26 (1.05: >0.96)	1.26 (1.05: >0.86)	0.98 (1.07: 0.78–1.32)
(SIS1)	1.40 (1.11: >1.27)	1.40 (1.10: >1.23)	1.31 (1.10: >1.07)
(SIS0&1)	1.40 (1.05: >1.24)	1.40 (1.05: >1.17)	1.19 (1.08: 1.00–1.36)
(GIS&SIS)	1.33 (1.03: >1.22)	1.31 (1.03: >1.13)	1.15 (1.05: 1.02–1.27)
Ginga			
	1.28 (0.46: >1.17)	1.23 (0.46: 1.08–1.38)	1.19 (1.19: 1.06–1.32)
Hellier (1)		0.91–1.29	
Hellier (2)		0.74–1.14	
Refining	1 & 2	0.78–1.03	

determinations for lower mass white dwarfs remain largely-unaffected.

Comparing the revised determinations with those from other methods, we note that agreement in the case of XY Ari is significantly improved: for the *RXTE* data the best mass and 2σ errors are in close agreement with those determined from the eclipse duration in Ramsay et al. (1998). The *Ginga* and *ASCA* determinations remain significantly higher, however: Ramsay et al. (1998) explored some of the possible explanations for this. In the case of the systems in Table 1 for which other determinations exist (see also Cropper et al. 1998), we note close agreement in the case of the lower mass systems EX Hya as determined from the X-ray line data (Fujimoto & Ishida 1997; Ezuka & Ishida 1999), and with AO Psc and TX Col (Hellier et al. 1996; Ezuka & Ishida 1999). In the case of FO Aqr, where the mass is higher at $\sim$1 $M_\odot$, there is also close agreement with that determined from *ASCA* data (Ezuka & Ishida 1999). The *Ginga* data for AE Aqr and QQ Vul are relatively poorer, and do not constrain the masses strongly: both are nevertheless consistent with those determined elsewhere (Mukai & Charles 1987; Welsh, Horne & Gomer 1995). Only in the case of AM Her is the mass we derive still significantly higher than those from other techniques (Gänsicke et al. 1998, and to a lesser extent, Mukai & Charles 1987). However, the effect of the absorption model is particularly strong, so that if a partial covering model is assumed, even here the mass of 0.85 $M_\odot$ is not controversially high (Mukai & Charles 1987).

We note that any technique for determining the mass of the white dwarf will have both systematic biases built into the method and uncertainties arising from poor constraints in some of the input parameters, such as inclination for the kinematically derived masses, or perhaps instrumental effects as in the case of XY Ari (Ramsay et al. 1998).

Our results indicate the importance of the absorption model on the mass determinations. The effect can be minimized by excluding the softest photons from the fits to the data, especially in the case of CCD data with sufficient spectral resolution. The resulting models can be used retrospectively to isolate the absorption at lower energies. Clearly, with shock temperatures in excess of 40 keV for 1-$M_\odot$ white dwarfs, X-ray spectra with sufficient data quality extending to approximately equivalent energies are beneficial for the extraction of mass information.

ACKNOWLEDGMENTS

We are very grateful to Lee McDonald and Mitchell Berger for their help, and to Andy Beardmore who pointed out the need to use cosmic abundances to determine the shock temperature appropriately. KW acknowledges the support from the Australian Research Council through an an Australian Research Fellowship.

REFERENCES

Aizu K., 1973, Prog. Theor. Phys., 49, 1184
Chanmugam G., Wu K., Courtney M. W., Barrett P. E., 1989, ApJS, 71, 323
Cropper M., 1990, Space Sci. Rev., 54, 195
Cropper M., Ramsay G., Wu K., 1998, MNRAS, 293, 222
Cropper M., Wu K., Ramsay G., 1999, in Hellier C., Mukai K., eds, ASP Conf. Ser., Proc. 2nd Workshop on Magnetic Cataclysmic Variables, Annapolis, July 1998, Astron. Soc. Pac., San Francisco, 157, 325
Done C., Magdziarz P., 1998, MNRAS, 298, 737
Ezuka H., Ishida M., 1999, preprint
Frank J., King A. R., Raine D., 1992, Accretion Power in Astrophysics. Cambridge Univ. Press, Cambridge, 2nd edition
Fujimoto R., Ishida M., 1997, ApJ, 474, 774
Gänsicke B., Hoard D. W., Beuermann K., Sion E. M., Szkody P., 1998, A&A, 338, 933
Hellier C., Mukai K., Ishida M., Fujimoto R., 1996, MNRAS, 280, 877
Imamura J. N., Durisen R. H., 1983, ApJ, 268, 291
Mukai K., Charles P., 1987, MNRAS, 226, 209
Ramsay G., Cropper M. S., Hellier C., Wu K., 1998, MNRAS, 297, 1269
Wada T., Shimizu A., Suzuki M., Kato M., Hoshi R., 1980, Prog. Theor. Phys., 64, 1986
Warner B., 1995, Cataclysmic Variable Stars. Cambridge Univ. Press, Cambridge
Welsh W. F., Horne K., Gomer R., 1995, MNRAS, 275, 649
Woelk U., Beuermann K., 1996, A&A, 306, 232
Wu K., 1994. Proc. Astron. Soc. Aust., 11, 61
Wu K., Chanmugam G., Shaviv G., 1994, ApJ, 426, 664

APPENDIX A: HYDRODYNAMIC EQUATIONS

The time-dependent mass continuity, momentum and energy equations are (see, e.g., Frank, King & Raine 1992):

$$\frac{\partial \rho}{\partial t} + \nabla\cdot(\rho \boldsymbol{v}) = 0, \tag{A1}$$

$$\rho \frac{\partial \boldsymbol{v}}{\partial t} + \rho \boldsymbol{v}\cdot\nabla \boldsymbol{v} = -\nabla \boldsymbol{P} + \boldsymbol{f} \tag{A2}$$

$$\frac{\partial}{\partial t}\left(\frac{1}{2}\rho v^2 + \rho\varepsilon\right) + \boldsymbol{\nabla}\cdot\left[\left(\frac{1}{2}\rho v^2 + \rho\varepsilon + P\right)\boldsymbol{v}\right] = \boldsymbol{f}\cdot\boldsymbol{v} - \nabla\cdot\boldsymbol{F}_{\rm rad}\ . \tag{A3}$$

Here we ignore heat conduction and fluid viscosity.

A1 The radiative cooling

By Gauss's Theorem, we can replace the volume integral of the divergence of the radiation flux $\nabla\cdot\boldsymbol{F}_{\rm rad}$ in (A3) by a surface integral

$$\int {\rm d}^3x\ \nabla\cdot\boldsymbol{F}_{\rm rad}\ = \oint {\rm d}\boldsymbol{s}\ \cdot\boldsymbol{F}_{\rm rad}$$

Suppose that the radiative flux $\boldsymbol{F}_{\rm rad}$ consists of two components: an optically thin bremsstrahlung term $\boldsymbol{F}_{\rm br}$ and an optically thick cyclotron term $\boldsymbol{F}_{\rm cyc}$; thus

$$\boldsymbol{F}_{\rm rad} = \boldsymbol{F}_{\rm br} + \boldsymbol{F}_{\rm cyc}.$$

Since bremsstrahlung emission is optically thin and isotropic, the surface integral of its flux at any arbitrary closed surface S' is 4π times the volume integral of the bremsstrahlung emissivity in a volume V' enclosed by the surface. Therefore we have

$$\oint_{S'} {\rm d}\boldsymbol{s}\cdot\boldsymbol{F}_{\rm br}\ = \int_{V'} {\rm d}^3x\ (4\pi j_{\rm br})\ = \int_{V'} {\rm d}^3x\ \Lambda_{\rm br}\ ,$$

where $\Lambda_{\rm br}$ is the energy loss per unit volume due to bremsstrahlung emission, which is the bremsstrahlung cooling function. Since the volume V' is arbitrarily chosen, we have in all space

$$\nabla\cdot\boldsymbol{F}_{\rm br} = \Lambda_{\rm br} = A\rho^2\sqrt{\frac{P}{\rho}}\ ,$$

where A is the constant for bremsstrahlung emission, P is the pressure, and ρ is the density.

To evaluate the volume integral of the divergence of the cyclotron flux, we consider the post-shock emission region as a cylinder with its symmetry axis parallel to the magnetic field. Because cyclotron emission is not optically thin and is not isotropic, we cannot equate

$\nabla\cdot\boldsymbol{F}_{\rm cyc}/4\pi$ to the cyclotron emissivity $j_{\rm cyc}$. As the volume integral of the divergence of the flux is the same as the integration of the flux over the surface enclosing the volume, we need only to evaluate the flux at the surface of the cylinder. Cyclotron emission is strongly beamed such that most power propagates preferentially in the direction perpendicular to the magnetic field, the vector products of $\mathrm{d}\boldsymbol{s}\cdot\boldsymbol{F}_{\rm cyc}$ at the top surface S_1 and the bottom surface S_3 of the cylinder are small in comparison with that at the side surface S_2 (this is not equivalent to assuming that the fluxes at the surfaces S_1 and S_3 are small). As an approximation, we neglect their contribution to the surface integral. Then we have

$$\int_{V_{\rm c}} \mathrm{d}^3x\ \nabla\cdot\boldsymbol{F}_{\rm cyc}\ \simeq \int_{S_2} \mathrm{d}\boldsymbol{s}\cdot\boldsymbol{F}_{\rm cyc}\ ,$$

where $V_{\rm c}$ is the total volume of the cylinder.

Suppose the spectrum of the cyclotron emission is optically thick up to a frequency $\nu_*(=\omega_*/2\pi)$ after which it is optically thin. For parameters typical of the accretion shocks in mCVs the optically thin cyclotron intensity falls rapidly with frequency as $\sim\nu^{-8}$ (see Chanmugam et al. 1989). As a first approximation, we can neglect the contribution of the optically thin cyclotron emission to the total cyclotron cooling process determining the structure of the post-shock accretion flow. Thus

$$\int_{S_2} \mathrm{d}\boldsymbol{s}\cdot\boldsymbol{F}_{\rm cyc} \simeq \pi^2 D \int_{R_{\rm WD}}^{x_{\rm s}} \mathrm{d}x \int_0^{\nu_*} \mathrm{d}\nu B_{\rm RJ}(\nu),$$

where $B_{\rm RJ} = 2kT\nu^2/c^2$ is the Rayleigh–Jeans intensity, $x_{\rm s}$ is the shock height, and D is the diameter of the cylinder (which is the accretion column) respectively.

If we divide the accretion column in layers of height $\mathrm{d}x$, the cyclotron luminosity, which is the total energy loss due to cyclotron emission, is the sum of the contribution of these layers:

$$L_{\rm cyc} = \int_{R_{\rm WD}}^{x_{\rm s}} \mathrm{d}x\ \frac{\mathrm{d}L_{\rm cyc}}{\mathrm{d}x}\ .$$

Thus we obtain an effective local cyclotron cooling term

$$\Lambda_{\rm cyc} = \frac{\mathrm{d}L_{\rm cyc}}{\mathrm{d}x} = \pi D \frac{kT\omega_*^3}{12\pi^2c^2}\ .$$

Now, from Wada et al. (1980),

$$\omega_*(x) \simeq 9.87\omega_{\rm c}\left(\frac{\Theta}{10^4}\right)^{0.05}\left(\frac{T}{10^8\mathrm{K}}\right)^{0.5},$$

where the cyclotron frequency $\omega_{\rm c} = eB/m_{\rm e}c$, and the dimensionless plasma parameter $\Theta = 2\pi n_{\rm e}(x)D/B$ (normally written Λ). Here B is the magnetic field, and $n_{\rm e}$ is the electron number density. For constant B,

$$\Lambda_{\rm cyc} \propto \omega_*^3 T \propto n_{\rm e}^{0.15} T^{2.5}.$$

We define two quantities:

$$t_{\rm cyc} \equiv \frac{3}{2}(n_{\rm e}+n_{\rm i})kT\frac{1}{\Lambda_{\rm cyc}}$$

and

$$t_{\rm br} \equiv \frac{3}{2}(n_{\rm e}+n_{\rm p})kT\frac{1}{\Lambda_{\rm br}}$$

for the cyclotron and bremsstrahlung cooling respectively ($n_{\rm i}$ is the ion number density). In terms of these two quantities, the total effective cooling term is

$$\Lambda = \Lambda_{\rm br} + \Lambda_{\rm cyc} = \Lambda_{\rm br}\left(1+\frac{t_{\rm br}}{t_{\rm cyc}}\right)$$

with

$$\frac{t_{\rm br}}{t_{\rm cyc}} \propto \frac{T^2}{n_{\rm e}^{1.85}}\ .$$

We assign a proportionality $\epsilon(x) = t_{\rm br}/t_{\rm cyc}$, and scale it in terms of the pressures and densities at the shock, $\epsilon_{\rm s}$. With the ideal-gas law, we eliminate the temperature and obtain

$$\epsilon(x) = \frac{t_{\rm br}}{t_{\rm cyc}}\bigg|_{x_{\rm s}}\left(\frac{P}{P_{\rm s}}\right)^{2.0}\left(\frac{\rho_{\rm s}}{\rho}\right)^{3.85}.$$

Thus we arrive at the effective cooling term determining the dynamics of the flow as that used in Wu (1994)

$$\Lambda = \Lambda_{\rm br}\left[1+\epsilon_{\rm s}\left(\frac{P}{P_{\rm s}}\right)^{2.0}\left(\frac{\rho_{\rm s}}{\rho}\right)^{3.85}\right]. \tag{A4}$$

A2 Steady state 1D hydrodynamic equations including gravity

For a stationary state, the time-derivative in the hydrodynamic equations are zero. As we consider a 1D flow channelled along a cyclinder parallel to the magnetic field, (A1) to (A3) can be reduced to

$$\frac{\mathrm{d}}{\mathrm{d}x}(\rho v) = 0, \tag{A5}$$

$$\rho v\frac{\mathrm{d}v}{\mathrm{d}x} + \frac{\mathrm{d}P}{\mathrm{d}x} = f, \tag{A6}$$

$$\frac{\mathrm{d}}{\mathrm{d}x}[(\frac{1}{2}\rho v^2 + \rho\varepsilon + P)v] = vf - \Lambda. \tag{A7}$$

The symbols are as defined in Section 2; f is the force term, and ε is the internal energy of the gas. As the cross-section of the accretion column is small in comparison with the white dwarf radius, it is adequate to let

$$f = \rho g = -\frac{\rho GM}{x^2}\ .$$

Noting from (A5) that

$$\frac{\mathrm{d}}{\mathrm{d}x}(\rho v^2) = v\frac{\mathrm{d}}{\mathrm{d}x}(\rho v) + \rho v\frac{\mathrm{d}v}{\mathrm{d}x} = \rho v\frac{\mathrm{d}v}{\mathrm{d}x},$$

we obtain for (A6)

$$\frac{\mathrm{d}}{\mathrm{d}x}(\rho v^2 + P) = -\rho\frac{GM}{x^2}\ . \tag{A8}$$

Substituting for f from (A6) in (A7) yields

$$v\frac{\mathrm{d}}{\mathrm{d}x}(\rho\varepsilon - \frac{1}{2}\rho v^2) + (\frac{1}{2}\rho v^2 + \rho\varepsilon + P)\frac{\mathrm{d}v}{\mathrm{d}x} = -\Lambda.$$

Using $\varepsilon = \frac{P}{\rho}\frac{1}{\gamma-1}$, and again (A5), we obtain

$$\frac{v}{\gamma-1}\frac{\mathrm{d}P}{\mathrm{d}x} + \frac{\gamma P}{\gamma-1}\frac{\mathrm{d}v}{\mathrm{d}x} = -\Lambda,$$

and thus

$$v\frac{\mathrm{d}P}{\mathrm{d}x} + \gamma P\frac{\mathrm{d}v}{\mathrm{d}x} = -(\gamma-1)\Lambda; \tag{A9}$$

in (A5), (A8) and (A9) we recover the hydrodynamic equations of Wu (1994), but with the additional gravitational force term in the momentum equation.

A3 Coupled first-order form

We now substitute the variable $\xi = v + (P/\rho v)$ in place of P in the

hydrodynamic equations. Thus the momentum equation (A8) becomes

$$\frac{\mathrm{d}}{\mathrm{d}x}(\rho v\xi) = \frac{-GM\rho}{x^2}.$$

Using (1) we obtain

$$\rho v\frac{\mathrm{d}\xi}{\mathrm{d}x} = \frac{-GM\rho}{x^2},$$

and thus

$$\frac{\mathrm{d}\xi}{\mathrm{d}x} = \frac{-GM}{x^2 v}. \tag{A10}$$

Substituting for ξ in the energy equation (A7) and noting from (A1) that $\rho v = \text{constant} = C$ (where $-C$ is the mass transfer rate $\dot{M}$),

$$vC\frac{\mathrm{d}\xi}{\mathrm{d}x} - vC\frac{\mathrm{d}v}{\mathrm{d}x} + \gamma C(\xi - v)\frac{\mathrm{d}v}{\mathrm{d}x} = -(\gamma - 1)\Lambda\ .$$

Thus

$$\frac{\mathrm{d}v}{\mathrm{d}x} = \frac{-\frac{\gamma-1}{C}\Lambda + \frac{GM}{x^2}}{\gamma(\xi - v) - v}. \tag{A11}$$

Now, substituting for Λ_{br} in (A4), we have

$$\Lambda = A\rho^2\sqrt{\frac{P}{\rho}}\left[1 + \epsilon_{\mathrm{s}}\left(\frac{P}{P_{\mathrm{s}}}\right)^{\alpha}\left(\frac{\rho_{\mathrm{s}}}{\rho}\right)^{\beta}\right];$$

thus

$$\Lambda = \frac{AC^2}{v^2}\sqrt{v(\xi - v)}\left[1 + \epsilon_{\mathrm{s}}\frac{4^{\alpha+\beta}}{3^{\alpha}}\frac{(\xi - v)^{\alpha}v^{\beta}}{v_{\mathrm{a}}^{\alpha+\beta}}\right], \tag{A12}$$

where we have used zero pre-shock pressure [so that across the shock from (2) $\rho_{\mathrm{a}}v_{\mathrm{a}}^2 = \rho_{\mathrm{s}}v_{\mathrm{s}}^2 + P_{\mathrm{s}}$ and $\rho_{\mathrm{a}}v_{\mathrm{a}} = \rho_{\mathrm{s}}v_{\mathrm{s}}$] to eliminate P_{s} and ρ_{s}, and the symbols are defined in Section 2. Combining (A10) to (A12), we obtain equations (4) and (5) in Section 2.

A4 Second-order form

We now proceed to the second-order form in v. We eliminate ξ by substituting further $w = (\xi/v) - 1$ and

$$\epsilon_{\mathrm{s}}' = \epsilon_{\mathrm{s}}\frac{4^{\alpha+\beta}}{3^{\alpha}}\frac{1}{v_{\mathrm{a}}^{\alpha+\beta}}.$$

Equation (4) becomes

$$\frac{\mathrm{d}x}{\mathrm{d}v} = \frac{v(\gamma w - 1)}{-(\gamma - 1)\frac{AC}{v}\sqrt{w}\left(1 + \epsilon_{\mathrm{s}}'v^{5.85}w^2\right) + \frac{GM}{x^2}}. \tag{A13}$$

For $\epsilon_{\mathrm{s}}' = 0$ (no cyclotron) this is a quadratic in $\sqrt{w}$ and two roots can be found analytically by rearranging (A13) and applying the standard formula for quadratic roots. Otherwise this is a quintic with no general analytic form for the roots, which then have to be found numerically for the particular case.

Differentiating (A13) again we have

$$\frac{\mathrm{d}^2x}{\mathrm{d}v^2} = \frac{\left\{\left[-(\gamma - 1)\frac{AC\sqrt{w}}{v^2} + \frac{GM}{x^2v}\right]\gamma\frac{\mathrm{d}w}{\mathrm{d}v} - (\gamma w - 1)\left[-(\gamma - 1)\frac{AC}{v^2}\left(\frac{1}{2\sqrt{w}}\frac{\mathrm{d}w}{\mathrm{d}v} - \frac{2\sqrt{w}}{v}\right) - \frac{GM}{x^2v}\left(\frac{2}{x}\frac{\mathrm{d}x}{\mathrm{d}v} + \frac{1}{v}\right)\right]\right\}}{\left[-(\gamma - 1)\frac{AC\sqrt{w}}{v^2} + \frac{GM}{x^2v}\right]^2}, \tag{A14}$$

where, from (5),

$$\frac{\mathrm{d}w}{\mathrm{d}v} = -\frac{GM}{x^2v^2}\frac{\mathrm{d}x}{\mathrm{d}v} - \frac{w + 1}{v}. \tag{A15}$$

Thus, by substituting for $\sqrt{w}$ from the roots of (A13), and $\mathrm{d}w/\mathrm{d}v$ from (A15) into (A14), we obtain a second-order, non-linear ODE in x and v alone.

This paper has been typeset from a TEX/LATEX file prepared by the author.